

CALIFORNIA UNIV BERKELEY DEPT OF MECHANICAL ENGINEERING F/G 20/4
 SUPERCRITICAL FLOW PAST SYMMETRICAL AIRFOILS.(U)
 DEC 80 K LI AFOSR-80-0230

AFOSR-TR-80-1357

NIL

END
DATE
FILMED
1-81
DTIC

AD A093300

LEVEL II ②

Supercritical Flow Past Symmetrical
Airfoils

by

Kon-Ming Li

Ph.D. Thesis
University of California, Berkeley
December 1980

SECURITY CLASSIFICATION OF THIS REPORT **UNCLASSIFIED**

REPORT DOCUMENTATION PAGE		READ INSTRUCTIONS BEFORE COMPLETING FORM	
1. REPORT NUMBER (18) AFOSR-TR-80-1357	2. GOVT ACCESSION NO. AD A093300	3. RECIPIENT'S CATALOG NUMBER	
4. TITLE (and Subtitle) (6) SUPERCRITICAL FLOW PAST SYMMETRICAL AIRFOILS.		5. TYPE OF REPORT & PERIOD COVERED (9) INTERIM rept.	
7. AUTHOR(s) (10) KON-MING/LI		8. CONTRACT OR GRANT NUMBER(s) (15) ✓ AFOSR-80-0230	
9. PERFORMING ORGANIZATION NAME AND ADDRESS UNIVERSITY OF CALIFORNIA, BERKELEY DEPART OF MECHANICAL ENGINEERING BERKELEY CA 94720		10. PROGRAM ELEMENT, PROJECT, TASK AREA & WORK UNIT NUMBERS (16) 61102F 2307/A4 (17) A4	
11. CONTROLLING OFFICE NAME AND ADDRESS AIR FORCE OFFICE OF SCIENTIFIC RESEARCH BOLLING AFB DC 20332		12. REPORT DATE (11) December 1980	
14. MONITORING AGENCY NAME & ADDRESS (if different from Controlling Office) (12) 51		13. NUMBER OF PAGES 44	
		15. SECURITY CLASS. (of this report) UNCLASSIFIED	
		15a. DECLASSIFICATION DOWNGRADING SCHEDULE	
16. DISTRIBUTION STATEMENT (of this Report) Approved for public release; distribution unlimited			
17. DISTRIBUTION STATEMENT (of the abstract entered in Block 20, if different from Report)			
18. SUPPLEMENTARY NOTES			
19. KEY WORDS (Continue on reverse side if necessary and identify by block number) TRANSONIC FLOW SUPERCRITICAL FLOW FULL POTENTIAL EQUATIONS TWO-DIMENSIONAL FLOW TELENIN'S METHOD METHOD OF LINES			
20. ABSTRACT (Continue on reverse side if necessary and identify by block number) A numerical method is developed for computing steady supercritical flow about an ellipse at zero angle to attack. The flow is assumed to be two-dimensional, inviscid, isentropic, and irrotational. The free stream Mach number lies in the high subsonic range so that a shock wave occurs locally near the body. The full potential equations are solved by Telenin's Method and the Method of Lines. Smooth interpolating functions are assumed for the unknown flow variables in selected coordinate directions. The resulting set of ordinary differential equations is then integrated away from or along the body depending			

DD FORM 1 JAN 73 1473

EDITION OF 1 NOV 65 IS OBSOLETE

UNCLASSIFIED

SECURITY CLASSIFICATION OF THIS PAGE (When Data Entered)

400426

SECURITY CLASSIFICATION OF THIS PAGE (When Data Enter)

~~UNCLASSIFIED~~

upon whether the flow is smooth or discontinuous. Jump conditions of the governing equations are applied across the shock wave so that it is perfectly sharp. A doublet solution for flow past a closed body is used as the far field boundary condition. Supercritical flow calculations have been performed for ellipses with thickness ratio of 0.2 and 0.4 at various free stream Mach numbers. The present results are compared with the shock-capturing method, and good agreement is obtained.

Accession For		
NTIS GRA&I <input checked="" type="checkbox"/>		
DTIC TAB <input type="checkbox"/>		
Unannounced <input type="checkbox"/>		
Justification		
By _____		
Distribution/ _____		
Availability Codes		
Dist	Avail and/or Special	
A	14 12	

~~UNCLASSIFIED~~
SECURITY CLASSIFICATION OF THIS PAGE (When Data Enter)

Supercritical Flow Past Symmetrical Airfoils

by

Kon-Ming Li

Abstract

A numerical method is developed for computing steady supercritical flow about an ellipse at zero angle of attack. The flow is assumed to be two-dimensional, inviscid, isentropic, and irrotational. The free stream Mach number lies in the high subsonic range so that a shock wave occurs locally near the body.

The full potential equations are solved by Telenin's Method and the Method of Lines. Smooth interpolating functions are assumed for the unknown flow variables in selected coordinate directions. The resulting set of ordinary differential equations is then integrated away from or along the body depending upon whether the flow is smooth or discontinuous. Jump conditions of the governing equations are applied across the shock wave so that it is perfectly sharp. A doublet solution for flow past a closed body is used as the far field boundary condition.

Supercritical flow calculations have been performed for ellipses with thickness ratio of 0.2 and 0.4 at various free-stream Mach numbers. The present results are compared with the shock-capturing method, and good agreement is obtained.

AIR FORCE OFFICE OF SCIENTIFIC RESEARCH (AFSO)
NOTICE OF TRANSMITTAL TO DDC
This technical report has been reviewed and is
approved for public release IAW AFR 190-12 (7b).
Distribution is unlimited.
A. D. BLOSE
Technical Information Officer

Acknowledgments

I am particularly indebted to Professor M. Holt for his continuing encouragement, advice and support. In addition, I am grateful to Mr. Larry Wigton, who performed the shock-capturing calculations for comparisons with the present work. I would also like to thank Sheila Slavin for her expert typing of this thesis.

Finally, I thank my parents for giving me the opportunity to pursue a higher education and their continuing moral support during this research.

The work presented in this thesis was supported by the U.S. Air Force Office of Scientific Research under Grant No. AFOSR-80-0230.

Table of Contents

	<u>Page</u>
1.0 Introduction	1
2.0 Formulation of the Problem	5
2.1 Equations of Motion	6
2.2 Description of the Flow Field	9
3.0 Numerical Methods	11
3.1 Boundary Conditions	13
3.2 Jump Conditions	16
3.3 Singular Points	18
3.4 Implementation of the Numerical Scheme	20
3.4.1 Coarse Solution	22
3.4.2 Refined Solution Near the Body	23
3.4.3 Powell's Method	25
4.0 Results and Discussion	27
5.0 Conclusions	30
References	31
Figures	33

List of Figures

- Fig. 1 Elliptic coordinates in the first quadrant with foci located at $(\pm 1, 0)$.
- Fig. 2(a) Unstable supercritical shock free flow field. Upper half plane.
 (b) Typical supercritical flow field. Upper half plane.
- Fig. 3(a) Singular ellipse for first formulation.
 (b) Singular ellipse for second formulation.
- Fig. 4 Integration in region 1.
 (a) Integration in the physical plane.
 (b) Integration in the ξ, η plane.
- Fig. 5 Integration in region 2.
 (a) Integration in the physical plane.
 (b) Integration in the ξ, η plane.
- Fig. 6 Surface velocity distribution. $\delta = 0.4, M_\infty = 0.65$.
- Fig. 7 Surface velocity distribution. $\delta = 0.4, M_\infty = 0.66$.
- Fig. 8 Surface velocity distribution. $\delta = 0.4, M_\infty = 0.67$.
- Fig. 9 Surface velocity distribution. $\delta = 0.4, M_\infty = 0.68$.
- Fig. 10 Surface velocity distribution. $\delta = 0.2, M_\infty = 0.77$.
- Fig. 11 Boundary of local supersonic region. $\delta = 0.4, M_\infty = 0.66$.
- Fig. 12 Boundary of local supersonic region. $\delta = 0.2, M_\infty = 0.77$.

1.0 Introduction

Within the past decade there has been strong interest in transonic flow research. The fact that commercial jets often fly at transonic speeds makes it very desirable to have methods which can predict airfoil lift and drag in this flow regime.

The flow is called transonic if both subsonic and supersonic regions are present in the field. Although most airplanes fly at subsonic speeds, the local flow velocities often become supersonic at the top of the wing. In a typical transonic flow field, the embedded supersonic region is usually terminated by means of a shock wave.

The main difficulties in transonic flow calculations are due to the inherent nonlinearities of the equations governing transonic flow, and the fact that the equations change type within the solution domain, from elliptic in the subsonic region to hyperbolic in the supersonic region. In addition, special provision must be made to handle the embedded shock wave in the flow field.

There are three main categories of numerical methods for solving steady inviscid flow past an airfoil in the transonic regime. These are finite difference methods, the hodograph method and interpolation methods.

Finite difference techniques have received the most attention in transonic flow research in recent years and we now outline them briefly.

Magnus and Yoshihara [1970] first solved the unsteady Euler equations using an explicit second-order difference scheme.

Unfortunately, the method requires a very large amount of computation

time to achieve steady state conditions, and is therefore very expensive for practical calculations.

An alternative to the time dependent approach is the use of relaxation methods. Murman and Cole [1971] successfully solved the transonic small disturbance equations by introducing a mixed finite difference system. The direction of differencing is biased depending upon whether the flow is subsonic or supersonic. The truncation error of the difference scheme has the effect of artificial viscosity, so shock waves appear naturally during the course of calculation, although they are usually spread over 3-4 mesh points. The system of difference equations is solved by successive line relaxation, and the computed results agree well with experimental data for a circular arc airfoil.

The method was extended by Krupp and Murman [1972] to lifting airfoils and slender bodies. Steger and Lomax [1972] solved the full potential equations for lifting airfoils by successive line over-relaxation (SLOR). An interactive graphic terminal is used to change the values of circulation and relaxation parameters as the relaxation is proceeding. To account for flows not aligned to the coordinate system, Jameson [1974] introduced a rotated differencing scheme in which the direction of upwind differencing is rotated to conform with the local flow direction. The system of difference equations is then iterated by simulating an artificial time dependent equation.

Ballhaus, Jameson and Albert [1978] developed an implicit approximate factorization (AF) algorithm for the solution of steady state transonic small disturbance equation, which has a much better rate of convergence than the SLOR algorithm. Following the idea of Jameson's rotating upwind difference scheme, Holst and Ballhaus [1979] solved the full potential equation in conservation form to ensure conservative

shock capturing. Artificial viscosity is added implicitly by retarding the density according to local Mach number. Holst [1979] later applied the method using an arbitrary mesh, and obtained good agreement with independently computed results.

The hodograph method has a long history in transonic flow calculations, taking advantage of the property that the governing equations of plane motion become linear when coordinates in the physical plane are replaced by the velocity components as independent variables. Using the hodograph transformation, Nieuwland [1967] developed a technique for computing shock-free, symmetrical, supercritical flows about quasi-elliptic airfoil sections. The method was later extended by Boerstoeel [1967] to present a catalog of solutions for certain body shapes. Bauer, Garabedian and Korn [1972] also used the hodograph method to generate a shock-free flow with the corresponding boundary shapes.

The final category of the methods makes use of quasi-analytic techniques. These are the Method of Integral Relations (MIR), Telenin's method and the Method of Lines (see Holt [1977]). Each approach uses smooth interpolating functions to represent the unknown variables in a selected coordinate direction. The partial differential equations are thereby reduced to a set of ordinary differential equations along a set of rays in the flow field. The resulting equations are then solved as an initial value problem.

MIR was first applied by Chushkin [1957] for subsonic critical flow past an ellipse or ellipsoid. Later, Holt and Masson [1971] computed supercritical flow about a cylinder with the full potential equations. Tai [1974] also used MIR to solve the steady Euler equations for a lifting airfoil. Both of the above methods located a

shock point on the body, but no details about the shape of the shock in the interior of the flow field are obtained.

Chattot [1978] applied Telenin's Method in the hodograph plane for flow past a double wedge. A shock is fitted in the flow field to eliminate the limit lines. The complete shock location is obtained, but the method is restricted to a double wedge, where the boundaries in the hodograph plane are known in advance. Telenin's Method was also used by Gross and Holt [1975] to calculate critical and supercritical shock-free flow past ellipses.

In the present work supercritical flow past an ellipse at zero angle of attack is calculated. The steady two-dimensional full potential equations are solved by Telenin's Method and the Method of Lines. The jump conditions of the equations are used to fit a shock in the flow field to terminate the supersonic region. The formulation of the equations of motion and the details of the transonic flow field are discussed in Section 2. Applications of Telenin's Method and the Method of Lines to the supercritical flow problem are described in Section 3. Section 4 contains discussions of the supercritical calculations. The conclusions are presented in Section 5.

2.0 Formulation of the Problem

We consider the two-dimensional flow of a uniform stream past an ellipse. The free stream Mach number lies in the high subsonic range so that, while the flow in the region far from the ellipse is wholly subsonic, the flow field in the neighborhood of the ellipse is of mixed type with subsonic regions near the forward and rear stagnation points and a local supersonic region near the maximum thickness section of the ellipse. The local supersonic region is usually bounded by a shock wave at its downstream end. A typical flow pattern is shown in Fig. 2(b).

Viscosity effects are confined to the boundary layer near the surface of the ellipse. The boundary layer calculations will be carried out subsequently since these require knowledge of the inviscid flow field as a starting point. The shock terminating the local supersonic region causes the boundary layer to separate so that the inviscid and viscous flows interact significantly. However, the main influence of boundary layer separation is to introduce an effective thickening of the ellipse downstream of the shock. Interaction effects are therefore determined by integrating the inviscid and boundary layer equations separately and matching the calculations along the effective viscous-inviscid boundary.

The shock wave introduces entropy changes on its downstream side. Provided that the minor-major axis ratio (maximum thickness ratio) of the ellipse is sufficiently small and, provided that the free stream Mach number is subsonic, the local Mach number ahead of the shock wave will not exceed the value 1.3. The shock wave strength is then sufficiently small to ensure that entropy changes can be

neglected.

To verify this statement we use the following perfect gas relationship to determine entropy changes across a shock wave:

$$\frac{\Delta S}{R} = \frac{1}{\gamma-1} \ln \left[\frac{2\gamma M^2 - \gamma + 1}{\gamma + 1} \right] - \frac{\gamma}{\gamma-1} \ln \left[\frac{(\gamma+1)M^2}{(\gamma-1)M^2 + 2} \right] \quad (2.1)$$

Here, M is the incident Mach number (just upstream of the shock), γ the ratio of specific heats, R the gas constant, and ΔS the change in entropy. If $M = 1.3$ and $\gamma = 1.4$, then

$$\frac{\Delta S}{R} = 0.0208 \quad (2.2)$$

Equation (2.1) can be rewritten as

$$P_2 = P_1 \left(\frac{\rho_2}{\rho_1} \right)^\gamma \left[\exp \left(\frac{\Delta S}{R} \right) \right]^{(\gamma-1)} \quad (2.3)$$

where p is the pressure and ρ the density. Subscripts 1 and 2 denote conditions ahead and behind the shock, respectively.

From Eq. (2.2)

$$\left[\exp \left(\frac{\Delta S}{R} \right) \right]^{(\gamma-1)} = 1.0084 \quad (2.4)$$

It follows that for shocks with incident Mach numbers $M < 1.3$ the error introduced by the isentropic assumption is about 0.8%. We can therefore assume, in the present analysis, that the flow field is isentropic and irrotational.

2.1 Equations of Motion

We consider steady, two-dimensional flow of a uniform air stream past an ellipse at high subsonic free stream Mach numbers. The flow is assumed to be inviscid and irrotational. The governing equations of motion are then

Continuity

$$\text{div}(\rho \vec{q}) = 0 \quad (2.5)$$

Irrotationality

$$\text{curl}(\vec{q}) = 0 \quad (2.6)$$

Writing these equations in elliptic coordinates:

$$\frac{\partial(\rho u h)}{\partial \xi} + \frac{\partial(\rho v h)}{\partial \eta} = 0 \quad (2.7)$$

$$\frac{\partial(v h)}{\partial \xi} - \frac{\partial(u h)}{\partial \eta} = 0 \quad (2.8)$$

The elliptic coordinates ξ and η are defined by (Milne-Thomson [1972]):

$$x = c \cosh \xi \cos \eta \quad (2.9)$$

$$y = c \sinh \xi \sin \eta \quad (2.10)$$

where x and y are Cartesian coordinates, c is a constant, u and v are the velocity components in the ξ and η directions, respectively, and h is the metric coefficient given by:

$$h = c(\sinh^2 \xi + \sin^2 \eta)^{1/2} \quad (2.11)$$

It can be shown that curves of constant ξ represent confocal ellipses and curves of constant η confocal hyperbolae. The foci of the ellipses or hyperbolae are located at $(\pm c, 0)$. Some curves of the elliptic coordinate system with $c = 1$ are plotted in Fig. 1.

The final equation to complete the set is Bernoulli's equation:

$$H + \frac{1}{2} q^2 = H_0 = \frac{1}{2} q_{\max}^2 \quad (2.12)$$

The quantity H is the enthalpy (per unit mass), q is the flow speed, q_{\max} the maximum steady expansion speed, and the subscript o denotes stagnation conditions. Equation (2.12) may be written

$$\frac{H}{H_o} = 1 - \left(\frac{q}{q_{\max}}\right)^2 \quad (2.13)$$

For a perfect gas with constant specific heats

$$H = \frac{\gamma p}{(\gamma-1)\rho} \quad (2.14)$$

By further assuming isentropic flow

$$p \propto \rho^\gamma \quad (2.15)$$

it follows that

$$\frac{H}{H_o} = \frac{p}{p_o} \cdot \frac{\rho_o}{\rho} = \left(\frac{\rho}{\rho_o}\right)^{\gamma-1} \quad (2.16)$$

Substituting Eq. (2.16) into (2.13) and solving for ρ/ρ_o we obtain

$$\frac{\rho}{\rho_o} = \left(1 - \left(\frac{q}{q_{\max}}\right)^2\right)^{1/\gamma-1} \quad (2.17)$$

The three equations (2.7), (2.8) and (2.17) are the three relations required to determine the three basic unknowns u, v and ρ .

We now express all variables in dimensionless form by dividing distances by c , velocities by q_{\max} , and the density by the stagnation density ρ_o . Retaining the same symbols for the non-dimensional variables, the equations of motion are

$$\frac{\partial(\rho u h)}{\partial \xi} + \frac{\partial(\rho v h)}{\partial \eta} = 0 \quad (2.18)$$

$$\frac{\partial(v h)}{\partial \xi} - \frac{\partial(u h)}{\partial \eta} = 0 \quad (2.19)$$

$$\rho = (1 - q^2)^{1/\gamma-1} = (1 - u^2 - v^2)^{1/\gamma-1} \quad (2.20)$$

and

$$h = (\sinh^2 \xi + \sin^2 \eta)^{1/2} \quad (2.21)$$

$$x = \cosh \xi \cos \eta \quad (2.22)$$

$$y = \sinh \xi \sin \eta \quad (2.23)$$

2.2 Description of the Flow Field

Before we proceed to solve the equations of motion, it is advantageous to understand the physical flow field and be able to choose an effective method to solve the problem.

At very low Mach numbers, the compressibility is very small, hence the flow can be assumed to be incompressible. The analytic solution for incompressible flow past an elliptic cylinder (Milne-Thomson [1972]) is given by

$$u = \frac{U_\infty}{h} e^{\xi_0} \cos \eta \sinh(\xi - \xi_0) \quad (2.24)$$

$$v = -\frac{U_\infty}{h} e^{\xi_0} \sin \eta \cosh(\xi - \xi_0) \quad (2.25)$$

where U_∞ is the free stream velocity and ξ_0 the ellipse representing the body of the cylinder. On the body, the normal component u of the velocity is zero, and the tangential velocity is given by Eq. (2.25). It can be seen that the flow accelerates from stagnation at the leading edge ($\eta = \pi$) to a maximum speed at the apex of the cylinder ($\eta = \pi/2$), and then decelerates back to stagnation at the trailing edge ($\eta = 0$). At zero angle of attack, the flow is symmetric about both the y -axis and the x -axis.

As the free stream Mach number is increased, compressibility effects become more important, and the compressible equations of

motion have to be solved. However, the flow behavior remains qualitatively the same if the flow is subsonic throughout the field. When the maximum local Mach number reaches the value 1.0, the flow is said to be critical. The free stream Mach number which produces such a flow is called the critical free stream Mach number.

For supercritical flow, a small supersonic region is embedded in the subsonic flow field. Although shock free supercritical flows can be produced, they are generally unstable (see Busemann [1949], Frankl [1950], Guderley [1953], Morawetz [1956,1957]) in the sense that a small perturbation of the body contour in the supersonic region leads to a flow that is discontinuous. This will be assumed the case for our transonic flow calculation. A typical transonic flow field is depicted in Fig. 2(b).

3.0 Numerical Methods

Telenin's Method and the Method of Lines are used as the numerical schemes to solve the equations of motion. The two methods are very similar. In Telenin's Method the variations of the variables in one coordinate direction are represented by some smooth interpolating functions. In our problem, symmetry conditions suggest the use of Fourier series of the form:

$$u(\xi, \eta) = \sum_{i=1}^N a_i(\xi) \cos(i-1)\eta \quad (3.1)$$

$$v(\xi, \eta) = \sum_{i=1}^{N-2} b_i(\xi) \sin i\eta \quad (3.2)$$

where N is the number of rays. Along the j th ray

$$u_j = u(\xi, \eta_j) = \sum_{i=1}^N a_i(\xi) \cos(i-1)\eta_j \quad (3.3)$$

The coefficient a_i can be obtained by inverting the matrix $\{\cos(i-1)\eta_j\}$,

$$a_i = \sum_{j=1}^N A_{ij} u_j \quad i = 1, \dots, N \quad (3.4)$$

where $\{A_{ij}\} = \{\cos(j-1)\eta_i\}^{-1}$. Equation (3.1) is differentiated to obtain the η derivatives, giving

$$\left(\frac{\partial u}{\partial \eta}\right)_\ell = \frac{\partial u(\xi, \eta_\ell)}{\partial \eta} = \sum_{i=1}^N a_i(\xi) (1-i) \sin(i-1)\eta_\ell \quad (3.5)$$

Substituting Eq. (3.4) into Eq. (3.5) yields

$$\left(\frac{\partial u}{\partial \eta}\right)_\ell = \sum_{i=1}^N \left(\sum_{j=1}^N A_{ij} u_j \right) (1-i) \sin(i-1)\eta_\ell \quad (3.6)$$

Interchanging the order of operation,

$$\left(\frac{\partial u}{\partial \eta}\right)_\ell = \sum_{j=1}^N \left(\sum_{i=1}^N A_{ij} (1-i) \sin(i-1)\eta_\ell \right) u_j = \sum_{j=1}^N F_{\ell j} u_j \quad (3.7)$$

Similarly, for the derivative of v

$$\left(\frac{\partial v}{\partial \eta}\right)_\ell = \sum_{j=1}^{N-2} G_{\ell j} v_j \quad \ell = 1, 2, \dots, N \quad (3.8)$$

where

$$F_{\ell j} = \sum_{i=1}^N A_{ij} (1-i) \sin(i-1) \eta_\ell \quad (3.9)$$

$$G_{\ell j} = \sum_{i=1}^{N-2} B_{ij} i \cos i \eta_\ell \quad (3.10)$$

$$\{B_{ij}\} = \{\sin i \eta_{j+1}\}^{-1} \quad (3.11)$$

In the Method of Lines, the η derivatives are approximated by finite differences. Three-point or five-point difference schemes are used depending on the order of accuracy required. The derivative representation has the same form as given by Eq. (3.7) with coefficients F_{ij} derived from Taylor series expansions. Hence in terms of the solution method and accuracy, we may consider the two methods to be equivalent.

It is convenient to have expressions for $\partial v / \partial \xi$ and $\partial u / \partial \xi$.

From Eq. (2.19)

$$v \frac{\partial h}{\partial \xi} + h \frac{\partial v}{\partial \xi} = u \frac{\partial h}{\partial \eta} + h \frac{\partial u}{\partial \eta} \quad (3.12)$$

Solving for $\partial v / \partial \xi$:

$$\frac{\partial v}{\partial \xi} = \frac{1}{h} \left(u \frac{\partial h}{\partial \eta} + h \frac{\partial u}{\partial \eta} - v \frac{\partial h}{\partial \xi} \right) \quad (3.13)$$

The definition of h implies that

$$\frac{\partial h}{\partial \xi} = \frac{\sinh 2\xi}{2h} \quad (3.14)$$

and

$$\frac{\partial h}{\partial \eta} = \frac{\sin 2\eta}{2h} \quad (3.15)$$

The above expressions are substituted into Eq. (3.13) to give:

$$\frac{\partial v}{\partial \xi} = \frac{\partial u}{\partial \eta} + \frac{u \sin 2\eta}{2h^2} - \frac{v \sinh 2\xi}{2h^2} \quad (3.16)$$

From Eqs. (2.18) and (2.20), we obtain

$$\frac{u}{h} \frac{\partial h}{\partial \xi} + \frac{\partial u}{\partial \xi} + \frac{u}{\rho} \frac{\partial \rho}{\partial \xi} = -\frac{1}{\rho h} \frac{\partial(\rho v h)}{\partial \eta} \quad (3.17)$$

and

$$\frac{1}{\rho} \frac{\partial \rho}{\partial \xi} = -\frac{2[u \frac{\partial u}{\partial \xi} + v \frac{\partial v}{\partial \xi}]}{(\gamma-1)(1-u^2-v^2)} \quad (3.18)$$

Substituting (3.18) into (3.17) and solving for $\partial u / \partial \xi$,

$$\frac{\partial u}{\partial \xi} = \frac{P_1}{Q_1} \quad (3.19)$$

where

$$P_1 = 2uv \left(\frac{\partial v}{\partial \xi} + \frac{\partial u}{\partial \eta} \right) + 2v^2 \frac{\partial v}{\partial \eta} - (\gamma-1)(1-u^2-v^2) \left(\frac{\partial v}{\partial \eta} + \frac{v \sin 2\eta}{2h^2} + \frac{u \sinh 2\xi}{2h^2} \right) \quad (3.20)$$

$$Q_1 = (\gamma-1)(1-v^2) - (\gamma+1)u^2 \quad (3.21)$$

Substitution of expressions (3.7) and (3.8) into Eqs. (3.16) and (3.19) results in a system of $(2 \times N - 2)$ ordinary differential equations that can be integrated simultaneously in the ξ direction, along N rays of constant η .

3.1 Boundary Conditions

Boundary conditions have to be prescribed in order to specify the problem uniquely. On the body, we require that normal velocity

be zero, that is

$$u = 0 \quad \text{for} \quad \xi = \xi_0 \quad (3.22)$$

where ξ_0 is the elliptic coordinate of the body. For flow past an elliptic cylinder at zero angle of attack, the flow field is symmetric about the x-axis, so

$$v = 0$$

and

$$\frac{\partial u}{\partial \eta} = 0 \quad \text{for} \quad \eta = 0 \text{ and } \pi \quad (3.23)$$

Finally, the flow approaches that of a uniform free stream at infinity:

$$u \rightarrow U_\infty \cos \eta$$

and

$$v \rightarrow -U_\infty \sin \eta \quad \text{as} \quad \xi \rightarrow \infty \quad (3.24)$$

However, in practice, it is more convenient to specify the far field boundary conditions at a finite distance from the body.

Following Murman and Cole [1971], an analytical solution for the far field is derived using transonic small disturbance theory. The basic transonic equation is

$$[K\phi_x - (\gamma+1)\phi_x^2/2]_x + \phi_{\tilde{y}\tilde{y}} = 0 \quad (3.25)$$

with the variables and parameters defined by:

$$\tilde{y} = \delta^{1/3} y \quad (3.26)$$

$$K = (1-M_\infty^2)/\delta^{2/3} \quad (3.27)$$

$$\frac{q_x}{U_\infty} = 1 + \delta^{2/3} q'_x + \dots \quad (3.28)$$

$$\frac{q_y}{U_\infty} = \delta q'_y + \dots \quad (3.29)$$

$$\left. \begin{aligned} q'_x &= \phi_x \\ q'_y &= \phi_{\tilde{y}} \end{aligned} \right\} \text{the perturbation velocities} \quad (3.30)$$

Here δ is the thickness ratio of the airfoil (or ellipse), M_∞ the free stream Mach number, q_x and q_y are the velocity components in the x and y directions, respectively.

We rewrite Eq. (3.25) in the form

$$L\phi \equiv K\phi_{xx} + \phi_{\tilde{y}\tilde{y}} = [(\gamma+1)/2](u^2)_x \quad (3.31)$$

Applying Green's formula for L in the upper half plane and allowing for a shock jump in the flow field, we obtain the basic integral equation

$$\begin{aligned} \phi(x, \tilde{y}) &= \frac{1}{\pi K^{1/2}} \int_{-1}^{+1} \frac{x-x'}{(x-x')^2 + K\tilde{y}^2} F(x') dx' \\ &+ \frac{\gamma+1}{2} \frac{1}{2\pi K^{1/2}} \iint_{-\infty}^{\infty} \frac{(x-x') \{q'_x(x', y')\}^2}{(x-x')^2 + K(\tilde{y}-y')^2} dx' dy' \end{aligned} \quad (3.32)$$

The far field is thus that of the usual doublet for a closed body

$$\phi(x, \tilde{y}) \approx \frac{D}{2\pi K^{1/2}} \frac{x}{(x^2 + K\tilde{y}^2)} + \dots \quad (3.33)$$

where

D = doublet strength

$$= 2 \int_{-1}^1 F(x) dx + \frac{\gamma+1}{2} \iint_{-\infty}^{\infty} \{q'_x(x, y)\}^2 dx dy \quad (3.34)$$

The doublet strength consists of the usual term proportional to

the airfoil volume and a nonlinear contribution, unknown in advance.

In the numerical procedure D has to be calculated as one of the unknowns of the problem. Differentiating Eq. (3.33),

$$q'_x = \frac{D}{2\pi K^{1/2}} \frac{(-x^2 + K\tilde{y}^2)}{(x^2 + K\tilde{y}^2)^2} \quad (3.35)$$

$$q'_y = -\frac{DK^{1/2}}{\pi} \frac{xy}{(x^2 + K\tilde{y}^2)^2} \quad (3.36)$$

The flow velocities expressed in the ξ and η directions are given by:

$$u = \frac{1}{h} (q_x \sinh \xi \cos \eta + q_y \cosh \xi \sin \eta) \quad (3.37)$$

$$v = \frac{1}{h} (-q_x \cosh \xi \sin \eta + q_y \sinh \xi \cos \eta) \quad (3.38)$$

Substitution of Eqs. (3.28) and (3.29) into (3.37) and (3.38) gives the necessary boundary conditions in the far field.

3.2 Jump Conditions

For transonic flow at sufficiently high subsonic free stream Mach number, the flow becomes supercritical. A region of local supersonic flow is developed over the maximum thickness region of the body and this is terminated on the downstream side by a shock wave. In the inviscid flow approximation, the shock wave is modeled by a jump discontinuity in the solution. To ensure uniqueness, we require that entropy increases across the shock wave. For the full potential approximation, the entropy change is assumed to be negligible. Uniqueness is attained by allowing only the existence of compression shocks, but not expansion shocks. The jump conditions for the full potential equations are different from the usual Rankine-Hugoniot relations, and can be derived by writing the equations of motion in conservation form. Applying the two-dimensional form of the divergence

theorem to Eqs. (2.18) and (2.19), we obtain

$$\langle \rho u h \rangle (d\eta)_s - \langle \rho v h \rangle (d\xi)_s = 0 \quad (3.39)$$

and

$$\langle v h \rangle (d\eta)_s + \langle u h \rangle (d\xi)_s = 0 \quad (3.40)$$

where $\langle \rangle$ denote a jump in the quantity across the shock and subscript s denotes an element in the shock surface. Equations (3.39) and (3.40) can be rewritten as

$$\langle \rho u h \rangle \eta'_s - \langle \rho v h \rangle = 0 \quad (3.41)$$

$$\langle v h \rangle \eta'_s + \langle u h \rangle = 0 \quad (3.42)$$

where

$$\eta'_s = \left(\frac{d\eta}{d\xi} \right)_s \text{ is the shock wave angle} \quad (3.43)$$

In Eqs. (3.41) and (3.42) h is the metric coefficient which depends only on the geometry of the coordinate system and is continuous throughout the field, hence can be eliminated from Eqs. (3.41) and (3.42). The final form of the jump conditions is then

$$\langle \rho u \rangle \eta'_s - \langle \rho v \rangle = 0 \quad (3.44)$$

$$\langle v \rangle \eta'_s + \langle u \rangle = 0 \quad (3.45)$$

Equations (3.44) and (3.45) represent, respectively, the conservation of mass flux and continuity of tangential velocity across the shock wave. The density ρ in Eq. (3.44) is given by Bernoulli's equation (2.20). Thus the jump conditions for the full potential equations are completely specified.

It is interesting to compare the shock-fitting and shock-capturing methods. In the finite difference treatment of supercritical flow, artificial viscosity is added to the differential equations as a result of the truncation errors generated by the difference equations. No explicit jump conditions are needed, provided that the equations are written in divergence form to conserve mass flux. Shock waves evolve naturally during the course of the calculation, although they usually spread over several mesh points. In principle, the shock wave can be made arbitrarily sharp by refining the mesh points near to it; however, this will slow down the rate of convergence considerably. By employing a shock-fitting technique, the jump conditions are satisfied exactly. The shock wave is perfectly sharp, hence no refinement is necessary. The drawback of this method is that the iteration may not converge if the initial guess of the shock location is too inaccurate.

3.3 Singular Points

In Section 3.0 we assumed a Fourier series representation in the η direction for the unknown flow quantities, and, as a result, derived a set of first order ordinary differential equations (Eqs. (3.16) and (3.19)) in the ξ direction. However, it is also possible to assume an analytic representation in the ξ direction and obtain a set of ordinary differential equations in the η direction. The advantages and disadvantages of each formulation will become apparent at a later stage.

For the latter formulation, we must derive expressions for $\partial u / \partial \eta$ and $\partial v / \partial \eta$. Rearranging Eqs. (2.18) and (2.19), and solving for $\partial v / \partial \eta$ and $\partial u / \partial \eta$, we obtain

$$\frac{\partial u}{\partial \eta} = \frac{\partial v}{\partial \xi} + \frac{v \sinh 2\xi}{2h^2} - \frac{u \sin 2\eta}{2h^2} \quad (3.46)$$

$$\frac{\partial v}{\partial \eta} = \frac{P_2}{Q_2} \quad (3.47)$$

where

$$P_2 = 2uv\left(\frac{\partial u}{\partial \eta} + \frac{\partial v}{\partial \xi}\right) + 2u^2 \frac{\partial u}{\partial \xi} - (\gamma-1)(1-u^2-v^2)\left(\frac{\partial u}{\partial \xi} + \frac{u \sinh 2\xi}{2h^2} + \frac{v \sin 2\eta}{2h^2}\right) \quad (3.48)$$

$$Q_2 = (\gamma-1)(1-u^2) - (\gamma+1)v^2 \quad (3.49)$$

When Eqs. (3.16) and (3.19) are examined in detail, it is observed that they have a saddle point singularity when the denominator Q_1 becomes zero, that is,

$$(\gamma-1)(1-v^2) - (\gamma+1)u^2 = 0 \quad (3.50)$$

after rearranging, we obtain

$$\frac{u^2}{\frac{\gamma-1}{\gamma+1}} + v^2 = 1 \quad (3.51)$$

which represents an ellipse in the u, v plane. From Bernoulli's equation:

$$q^2 = \frac{(\gamma-1)M^2}{2 + (\gamma-1)M^2} \quad (3.52)$$

so the non-dimensional critical velocity q^* is

$$q^{*2} = \frac{\gamma-1}{\gamma+1} \quad (3.53)$$

Substituting Eq. (3.53) into (3.51), the ellipse of singularities may be written as

$$\frac{u^2}{q^{*2}} + \frac{v^2}{1} = 1 \quad (3.54)$$

The singular ellipse and the sonic circle are both plotted in Fig. 3a. We can see that all points on the ellipse lie outside the sonic circle, except for $v = 0$, $u = \pm q^*$. For critical flow, only one point is on the sonic circle, namely $u = 0$, $v = \pm q^*$, therefore there are no singularities for a critical flow calculation when integrating away from the body. It is apparent that no singularities will be encountered even for supercritical flow calculations.

On the other hand, using the second formulation and integrating in the η direction, the denominator of Eq. (3.47) becomes zero when

$$(\gamma-1)(1-u^2) - (\gamma+1)v^2 = 0 \quad (3.55)$$

Hence the singular ellipse in the u, v plane is given by

$$u^2 + \frac{v^2}{q^{*2}} = 1 \quad (3.56)$$

which is shown in Fig. 3b. But any critical or supercritical flow has a point on the body with $u = 0$ and $v = -q^*$, which is a point on the ellipse given by (3.56). Therefore it is obvious that integration in the η direction always leads to at least one singularity at sonic points on or near the body.

3.4 Implementation of the Numerical Scheme

As discussed in the preceding section, saddle point singularities will arise if we assume interpolating functions in the ξ direction. Hence it will be appropriate to use the first formulation given in Section 3.0. Expressions (3.7) and (3.8) are substituted into Eqs. (3.16) and (3.19) to form a set of $(2 \times N - 2)$ simultaneous ordinary differential equations. At $\xi = \xi_0$, the flow tangency condition on

the body is given by Eq. (3.22). An initial estimate of values of the tangential velocities v_0 on the surface is made, and using these as initial data, the equations are integrated away from the ellipse $\xi = \xi_0$. A variable step, fifth-order Runge-Kutta method is used to integrate the differential equations. The integration is terminated at a distance sufficiently far away from the body, say $\xi = \xi_\infty$, which will be defined later. The velocities v calculated at ξ_∞ are then compared with the far field velocities given by Eq. (3.38). If the two sets of values differ, tangential velocities on the surface are then adjusted and the integration is repeated. The procedure is repeated until the far field solution converges. This can be done very efficiently by the use of Powell's method (Powell, 1964), which minimizes the sum of squares of the differences between the far field velocities by adjusting the surface velocities. The iteration is terminated when the sum satisfies the specified tolerance.

Gilinskii, Telenin and Tinyakov [1964] pointed out that solving a Dirichlet problem as a Cauchy problem is inherently unstable with respect to the prescribed data. This phenomenon is known as Hadamard instability. Jones and South [1972] also encountered Hadamard instability in applying the Method of Lines and found growth in error proportional to $\exp(N\xi)$, where N is the number of rays and ξ the direction of integration. As a consequence, the number of rays and the far field distance have to be restricted. However, if we wish to obtain a solution with reasonable accuracy, we must employ sufficient number of rays to represent the variables. The occurrence of a shock wave on the body makes it even more desirable to have a detailed representation near the body.

To overcome the above difficulties, we propose to solve the

problem in two stages. In the first stage, a very coarse representation of the variables is used, which enables us to integrate the equations away from the body to the far field without instability problems. A supercritical shock free flow is obtained from this calculation. However, as discussed in Section 2.2, shockless flows are known to be unstable and not likely to occur in practical situations. Hence, in our supercritical flow calculation, we always assume that the flow is discontinuous. In order to model the shock wave, we have to treat the region near the body in a different manner. The procedure for the different stages is described in the following sections.

3.4.1 Coarse Solution

In this stage, we assume Fourier series representation of the form (3.1) and (3.2) for u and v . For flow over an ellipse, we further notice that the flow is symmetric about the y -axis when the solution is smooth. Thus we can economize on the number of rays by assuming the series of the form:

$$u(\xi, \eta) = \sum_{i=1}^{N-1} a_i(\xi) \cos(2i-1)\eta \quad (3.57)$$

$$v(\xi, \eta) = \sum_{i=1}^{N-1} b_i(\xi) \sin(2i-1)\eta \quad (3.58)$$

So for the coarse solution, we only need to compute the flow in the second quadrant. Equations (3.16) and (3.19) are integrated simultaneously from ξ_0 to ξ_∞ . Boundary conditions are satisfied by using the procedure described in Section 3.4. At supercritical Mach number, a continuous flow with a small embedded supersonic zone is obtained, and is depicted in Fig. 2a.

3.4.2 Refined Solution Near the Body

Although the coarse solution does not have enough accuracy to resolve the shock wave which occurs near the body, it provides a fairly good representation of the flow field away from the body where the flow is smooth. The strategy here is to use a larger number of rays to represent the flow field close to the body, the coarse solution at an intermediate value of ξ , say ξ_i , is used as the outer boundary condition for the refined solution near the body. In this way, the distance in the ξ direction is kept small and a larger number of rays can be used without causing instabilities.

It is advantageous to integrate the equations in the η direction if we wish to fit a shock in the flow field. Following the idea of Fletcher [1975], we divide the region near the body into two parts. The forward part is enclosed by $\xi = \xi_0$, $\xi = \xi_i$, $\eta = \pi$, and $\eta = \eta_i$, and the rear portion by $\xi = \xi_0$, $\xi = \xi_i$, $\eta = \eta_i$ and $\eta = 0$, which we shall call region 1 and region 2, respectively. The configurations are shown schematically in Figs. 4 and 5. ξ_i is chosen such that the point (ξ_i, η_i) is at the top of the sonic line (see Fig. 2a). In our case, $\eta_i = \pi/2$.

In region 1, finite difference formulae of the form (3.7) and (3.8) are used to calculate the derivatives in the η direction. The ordinary differential equations (3.16) and (3.19) are integrated as in the coarse calculation. No boundary condition is required on $\eta = \pi/2$, since there is no influence from downstream in a supersonic region, smooth transition through the sonic line will be sufficient for uniqueness. Tangential velocities on the body are adjusted so that velocities v at ξ_i match those of the coarse calculation. Five rays have been used in this region without encountering stability

problems.

In region 2, derivatives in the ξ direction are calculated by finite difference formulae of the following form:

$$\left(\frac{\partial u}{\partial \xi}\right)_\ell = \sum_{i=1}^M E_{\ell i} u_i \quad (3.59)$$

$$\left(\frac{\partial v}{\partial \xi}\right)_\ell = \sum_{i=1}^M H_{\ell i} v_i \quad (3.60)$$

where M is the number of rays, $E_{\ell i}$ and $H_{\ell i}$ are matrices obtained by Taylor series expansion. Expressions (3.59) and (3.60) are substituted into Eqs. (3.46) and (3.47) to form a set of ordinary differential equations. At $\eta = \pi/2$, the converged solution from region 1 is used as the initial condition to integrate the equations from $\eta = \pi/2$ to $\eta = 0$. At $\eta = 0$, the symmetry condition $v = 0$ is imposed. However, in the supersonic region the flow has no forewarning of the downstream conditions and the flow will not be able to adjust to satisfy symmetry conditions at $\eta = 0$. Physically, the supersonic region is terminated by a shock wave, the subsonic region behind the shock wave is subsequently compressed to satisfy the boundary condition downstream. To account for the embedded shock wave, the equations are integrated to an intermediate value of η , say $\eta_s(\xi)$, across which jump conditions (3.44) and (3.45) are applied. The integration is then resumed and carried out until $\eta = 0$ is reached. Powell's method is used to adjust the shock location η_s until v becomes zero on $\eta = 0$. The location of the shock is specified by its location on the surface and the shock slope on other rays. It is known, a priori, that the local shock shape must be normal to the surface in order to preserve the boundary condition of zero normal flow at the surface.

By splitting the solution domain near the body into two parts, we

have been able to integrate the equations of motion in different directions. In the rear part we chose to integrate the equations in the η direction so that a shock can be fitted in the flow field. Since the flow is supersonic ahead of the shock and subsonic behind (at least when boundary layer interaction effects are not considered), no saddle point singularity is encountered, thus the integration can be carried out without difficulty. As a word of caution, we note that the shock wave does not extend all the way from the surface to $\xi = \xi_i$ (see Fig. 2b). If we use a large number of rays, the rays of constant ξ with values close to ξ_i will pass through the sonic line and will cause difficulty if we try to integrate through this line. Therefore care must be taken to ensure that no rays pass through the sonic line.

After a converged solution for region 2 is obtained, the doublet strength D will be re-calculated, and the whole procedure repeated. The solution is considered to have converged globally when the values of D at successive iterations agree to within the prescribed tolerance.

3.4.3 Powell's Method

To complete the description of our numerical scheme, we shall describe Powell's method briefly; a more detailed analysis can be found elsewhere (see Powell [1964]). The method minimizes

$$\sum_{i=1}^N \epsilon_i^2 \quad (3.61)$$

with respect to F_1, F_2, \dots, F_M ($M \leq N$), where the N functions ϵ_i are nonlinear functions of the M unknowns F_j . The method is essentially that of least square minimization in which $\sum \epsilon_i^2$ is minimized by making changes to F_j according to the direction δF given by

$$\sum_{j=1}^M \left\{ \sum_{k=1}^N \frac{\partial \epsilon_k}{\partial F_i} \frac{\partial \epsilon_k}{\partial F_j} \right\} \delta F_j = - \sum_{k=1}^N \epsilon_k \frac{\partial \epsilon_k}{\partial F_i}$$

$$i = 1, 2, \dots, M \quad (3.62)$$

New values of \underline{F} are given by

$$\underline{F} = \underline{F}_{old} + \lambda \underline{\delta F} \quad (3.63)$$

in which λ is chosen (by search) such that $\sum \epsilon_i^2$ is minimized along the direction $\underline{\delta F}$. During the search along $\underline{\delta F}$ to locate the minimum, functions ϵ_i have to be evaluated at different values of λ ; thus one can calculate the rate of change of ϵ_i along the direction $\underline{\delta F}$ at the new minimum point by finite differences. Powell shows how these partial derivatives can be used in conjunction with previous values of $\frac{\partial \epsilon_k}{\partial F_i}$ to determine values for the next step given by (3.62).

In principle the method guarantees convergence since a step is taken only when $\sum \epsilon_i^2$ decreases. It also has quadratic convergence provided one is sufficiently near the solution and $\epsilon_i = 0$ at the minimum.

4.0 Results and Discussion

The algorithm introduced in the previous section is evaluated in this section by presenting a range of numerically computed solutions. Ellipses with thickness ratio $\delta = 0.4$ and $\delta = 0.2$ are chosen for the test cases. Free-stream Mach numbers are assumed to be high enough so that a shock wave will always occur. Gross and Holt [1975] reported critical flow for $\delta = 0.4$ at $M_\infty = 0.587$. Symmetric, supercritical, shock-free flows were obtained up to $M_\infty = 0.644$. A range of free-stream conditions has been chosen for our computations. For thickness ratio $\delta = 0.4$, free-stream Mach numbers were chosen to be 0.65, 0.66, 0.67 and 0.68. For $\delta = 0.2$, $M_\infty = 0.77$. ξ_∞ is assumed to be 2.5, which was found to be sufficiently large by Gross and Holt [1975]. Three rays are used for the coarse calculation. When four rays are used, the solution tends to oscillate in the ξ direction at large ξ , which is due to the instability discussed in Section 3.4. For region 1 of the refined calculation, five rays are used without encountering instability problems. However, for region 2 of the refined calculation, only three rays can be used. Besides the instability problem, there are possible singular points in the ordinary differential equations depending on whether or not the rays pass through the sonic points. This is due to the fact that the shock does not extend all the way out to $\xi = \xi_i$, typically, the top of the shock is located at approximately two-thirds of the distance between ξ_0 and ξ_i . It follows that the use of more than three rays will cause at least one ray to pass through the sonic point, which is hazardous when integrating in the η direction.

The present results are compared with calculations using the

shock-capturing method of Holst [1979] and are shown in Figs. 6-10. For $\delta = 0.4$, at $M_\infty = 0.65, 0.66$ and 0.67 , the two methods agree very well with the shock locations on the body almost identical. The surface velocity profiles obtained by both methods show similar characteristics. The flow undergoes a small compression before the shock wave is encountered. Behind the shock, a small post shock expansion wave is observed, after which the flow is recompressed back to stagnation condition at the trailing edge. The two methods show the largest discrepancies near the shock wave; in all the three cases tested, Holst's method consistently obtains a higher maximum velocity on the body and shows a steeper pre-shock compression. At $M_\infty = 0.64$, a solution with an embedded shock wave could not be obtained by the present method. As can be seen in the solution at $M_\infty = 0.65$, the shock jump is very weak, and it is quite probable that symmetric shock-free flows exist for free-stream Mach numbers lower than 0.65 . However, using Holst's method, a solution with shock jump is obtained for $M_\infty = 0.64$. At $M_\infty = 0.68$, the solution shows a local Mach number of 1.61 ahead of the shock, the isentropic assumption at this Mach number will introduce an error of about 4.7% according to Eqs. (2.3) and (2.5). Hence any solutions obtained at or above this free-stream Mach number will be erroneous.

Due to the unstable nature of the present method, the round-off error grows as $\exp(N \cdot \xi)$, where N is the number of rays in the ξ direction. It is difficult to assess the accuracy of the method. Nevertheless, good agreement is obtained between the present method and the shock-capturing method. The present method takes about 3 seconds to execute on a CDC 7600, whereas Holst's method takes about 6 seconds for a mesh size of 90×40 .

Unfortunately, the present method does not guarantee convergence unless the initial guess is reasonably close to the converged solution. One remedy is to increase the free-stream Mach number by a small fraction at a time, say by 0.005, and then use the solution obtained for a previous Mach number as an initial guess. Otherwise, good judgment and trial and error are needed in providing a good initial guess.

5.0 Conclusions

A composite numerical scheme has been developed which is based in part on Telenin's Method and in part on the Method of Lines. The numerical method has been designed to solve for supercritical flow over an ellipse, when the free-stream Mach number is high enough to generate an embedded shock wave in the flow field. A fitting technique is used to determine this shock so that the Rankine-Hugoniot jump conditions are satisfied exactly across the shock wave.

Good agreement is obtained between the present method and the shock-capturing technique. Further improvement in the present method can be achieved by the introduction of non-symmetrical flow effects into the solution over the forward part of the ellipse. To this end, it is desirable to represent the far flow field solution in terms of distributed singularities along the major axis of the ellipse rather than in terms of singularities all located at the ellipse center.

References

- Ballhaus, W. F., Jameson, A. and Albert, J., "Implicit Approximate Factorization Schemes for the Efficient Solution of Steady Transonic Flow Problems," *AIAA Journal*, 16, 573-579, 1978.
- Bauer, F., Garabedian, P. and Korn, D., A Theory of Supercritical Wing Sections, with Computer Program and Examples, Vol. 66 in Lecture Notes in Economics and Mathematical Systems, Springer-Verlag, New York, 1972.
- Boerstoeel, J. W., "A Survey of Symmetrical Transonic Potential Flows Around Quasi-Elliptical Aerofoil Sections," *NRL TR T-136*, January 1967, National Aerospace Laboratory, Amsterdam, The Netherlands.
- Busemann, A., "The Drag Problem at High Subsonic Speeds," *Journal of Aeronautical Sciences*, 16, 337-344, 1949.
- Chattot, J. J., "Symmetrical Flow Past a Double Wedge at High Subsonic Mach Numbers," *J. Fluid Mechanics*, 86, 161-177, 1978.
- Chushkin, P. I., "Subsonic Flow of a Gas Past Ellipses and Ellipsoids," *Vychislitel'naya Matematika*, 2, 20-24, 1958.
- Fletcher, C. J., "GTT Method Applied to Cones at Large Angles of Attack," *Proceedings 4th Int. Conf. on Numerical Methods in Fluid Dynamics. Lecture Notes in Physics*, 35, 161-166, Springer-Verlag, Berlin-Heidelberg-New York, 1975.
- Frankl, F. I., "On the Formation of Shocks in Subsonic Flows With Local Supersonic Velocities," *NACA TM No. 1251*(translation), 1950.
- Gilinskii, S. M., Telenin, G. F. and Tinyakov, G. P., "A Method of Computing Supersonic Flow Around Blunt Bodies, Accompanied by a Detached Shock Wave," *Izv. Akad. Nauk, SSSR Mekh. Mash.*, 4, 9-28, 1964 (translated as *NASA TT F297*, 1965).
- Gross, M. B. and Holt, M., "Steady Supercritical Flow Past Ellipses," *IUTAM Symposium Transsonicum II*, Göttingen, Germany, 1975, 369-375 (Eds. K. Oswatitsch and D. Rues), Springer-Verlag, Berlin-Heidelberg-New York, 1976.
- Guderley, G., "Shocks in Subsonic-Supersonic Flow Patterns," *Advances in Applied Mechanics*, Vol. III, Academic Press, New York, 1953.
- Holst, T. L. and Ballhaus, W. F., "Fast, Conservative Schemes for the Full Potential Equation Applied to Transonic Flows," *AIAA Journal*, 17, 145-152, 1979.

- Holst, T. L., "Implicit Algorithm for the Conservative Transonic Full Potential Equation Using an Arbitrary Mesh," AIAA Journal, 17, 1038-1045, 1979.
- Holt, M., Numerical Methods in Fluid Dynamics, Springer Series in Computational Physics. Springer-Verlag, Berlin-Heidelberg-New York, 1977.
- Holt, M. and Masson, B. S., "The Calculation of High Subsonic Flow Past Bodies by the Method of Integral Relations," Proceedings of the Second International Conference on Numerical Methods in Fluid Mechanics (Ed. M. Holt), Vol. 8, Lecture Notes in Physics, Springer-Verlag, Berlin-Heidelberg-New York, 1971, 243-251.
- Jameson, A., "Iterative Solution of Transonic Flows Over Airfoils and Wings, Including Flows at Mach 1," Comm. Pure Appl. Math., 27, 283-309, 1974.
- Jones, D. C., South, J. C. and Klunker, E. B., "On the Numerical Solution of Elliptic Partial Differential Equations by the Method of Lines," J. Comp. Phys., 9, 496-527, 1972.
- Krupp, J. A. and Murman, E. M., "Computation of Transonic Flows Past Lifting Airfoils and Slender Bodies," AIAA Journal, 10, 880-881, 1972.
- Magnus, R., and Yoshihara, H., "Inviscid Transonic Flow Over Airfoils," AIAA Journal, 8, 2157-2162, 1970.
- Milne-Thomson, L. M., Theoretical Hydrodynamics, Macmillan Press, 1972.
- Morawetz, C., "On the Non-Existence of Continuous Transonic Flows Past Profiles," Comm. Pure Appl. Math., 9 and 10, 1956-1957.
- Murman, E. M. and Cole, J. D., "Calculation of Plane Steady Transonic Flows," AIAA Journal, 9, 114-121, 1971.
- Nieuwland, G. Y., "Transonic Potential Flow Around a Family of Quasi-Elliptical Aerofoil Sections," NRL TR T-172, National Aerospace Laboratory, Amsterdam, The Netherlands, July 1967.
- Powell, M. J. D., "A Method for Minimizing a Sum of Squares of Nonlinear Functions Without Calculating Derivatives," Computer J., 7, 303-307, 1964.
- Steger, J. L. and Lomax, H., "Transonic Flow About Two-Dimensional Airfoils by Relaxation Procedures," AIAA Journal, 10, 49-54, 1972.
- Tai, T. C., "Transonic Inviscid Flow Over Lifting Airfoils by the Method of Integral Relations," AIAA Journal, 12, 798-804, 1974.

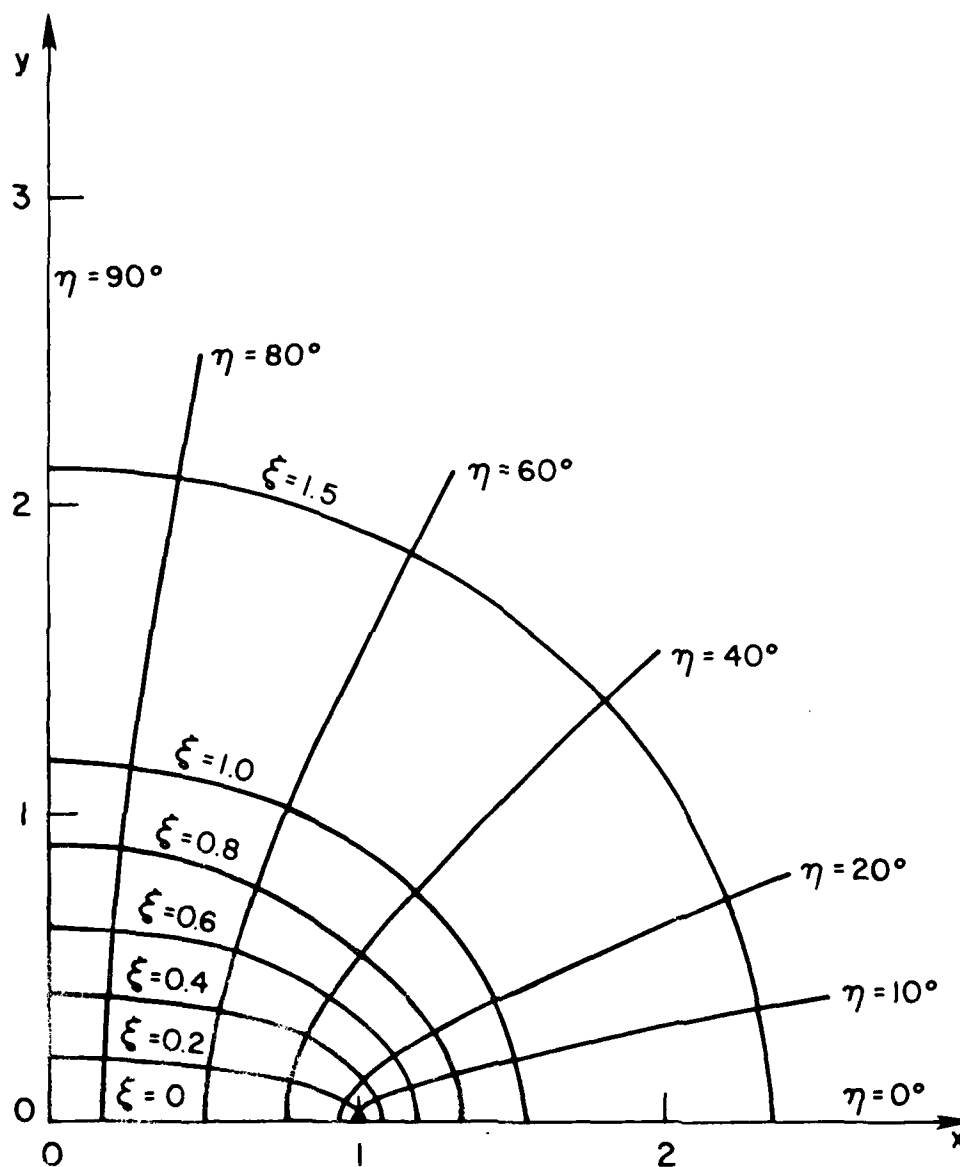


FIG. 1 ELLIPTIC COORDINATES IN THE FIRST QUADRANT
WITH FOCI LOCATED AT $(\pm 1, 0)$

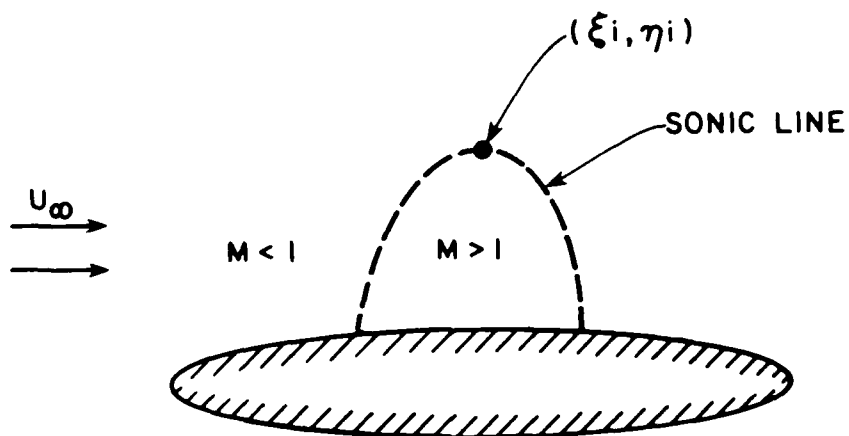


FIG. 2(a) UNSTABLE SUPERCRITICAL SHOCK FREE FLOW FIELD. UPPER HALF PLANE.

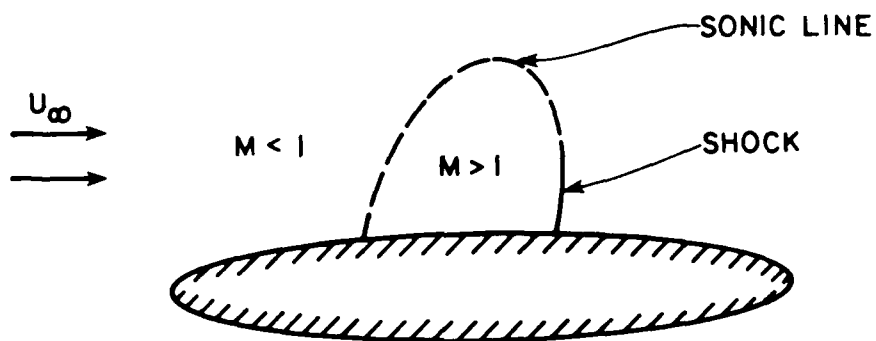


FIG. 2(b) TYPICAL SUPERCRITICAL FLOW FIELD. UPPER HALF PLANE.

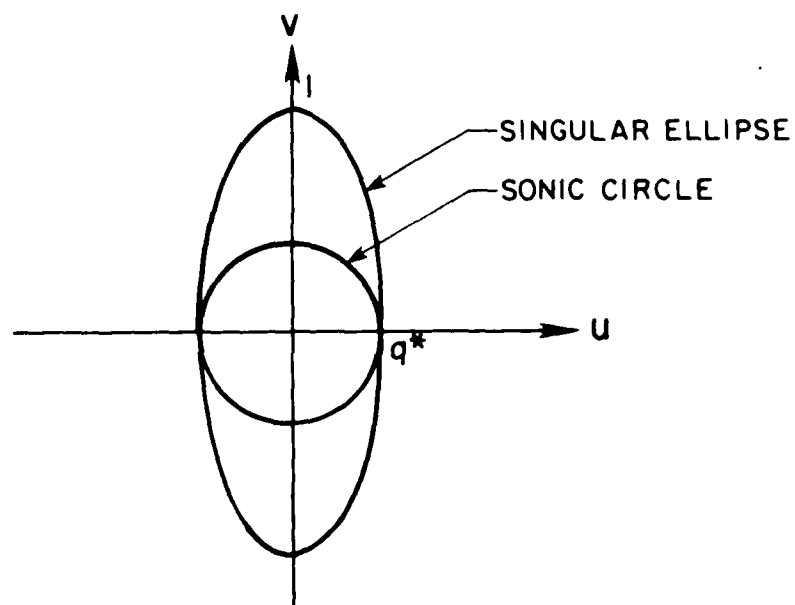


FIG. 3(a) SINGULAR ELLIPSE FOR FIRST FORMULATION.

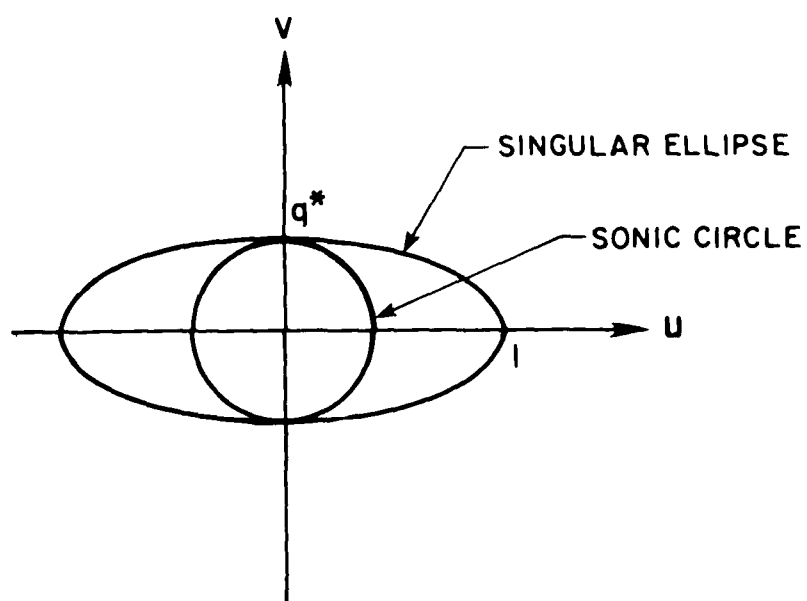
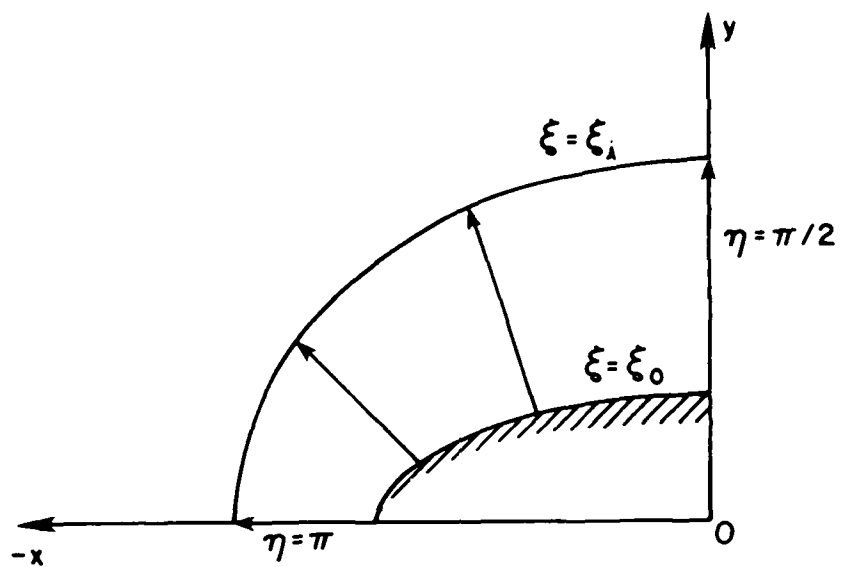
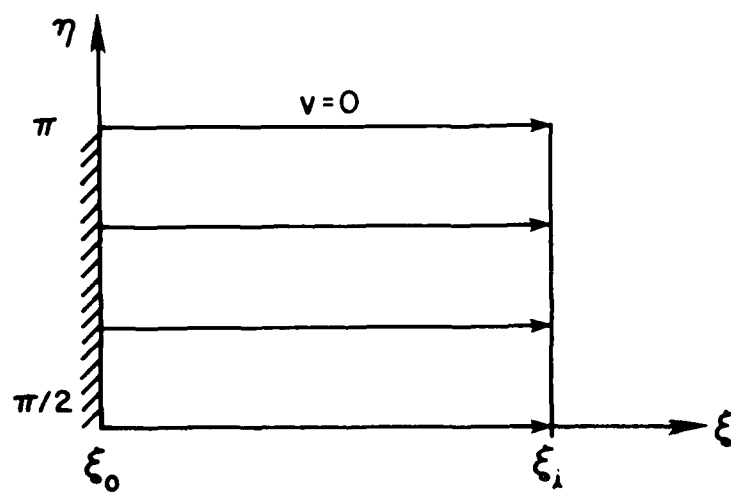


FIG. 3(b) SINGULAR ELLIPSE FOR SECOND FORMULATION.

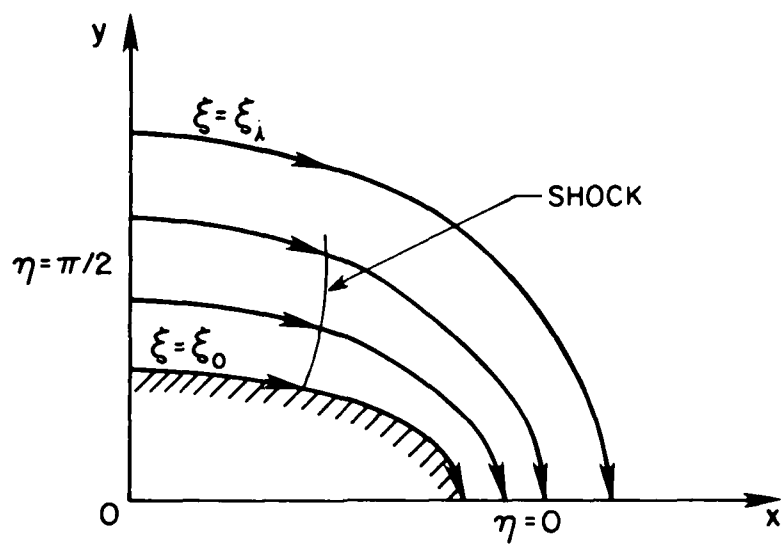


(a) INTEGRATION IN THE PHYSICAL PLANE.



(b) INTEGRATION IN THE ξ, η PLANE.

FIG. 4 INTEGRATION IN REGION 1



(a) INTEGRATION IN THE PHYSICAL PLANE.

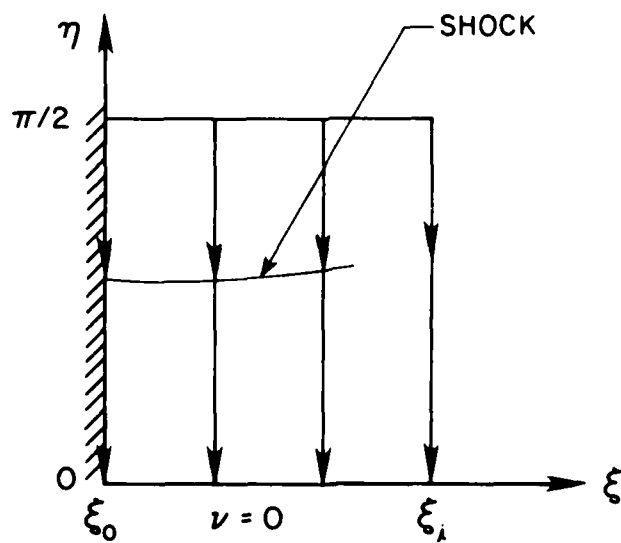
(b) INTEGRATION IN THE ξ, η PLANE.

FIG. 5 INTEGRATION IN REGION 2

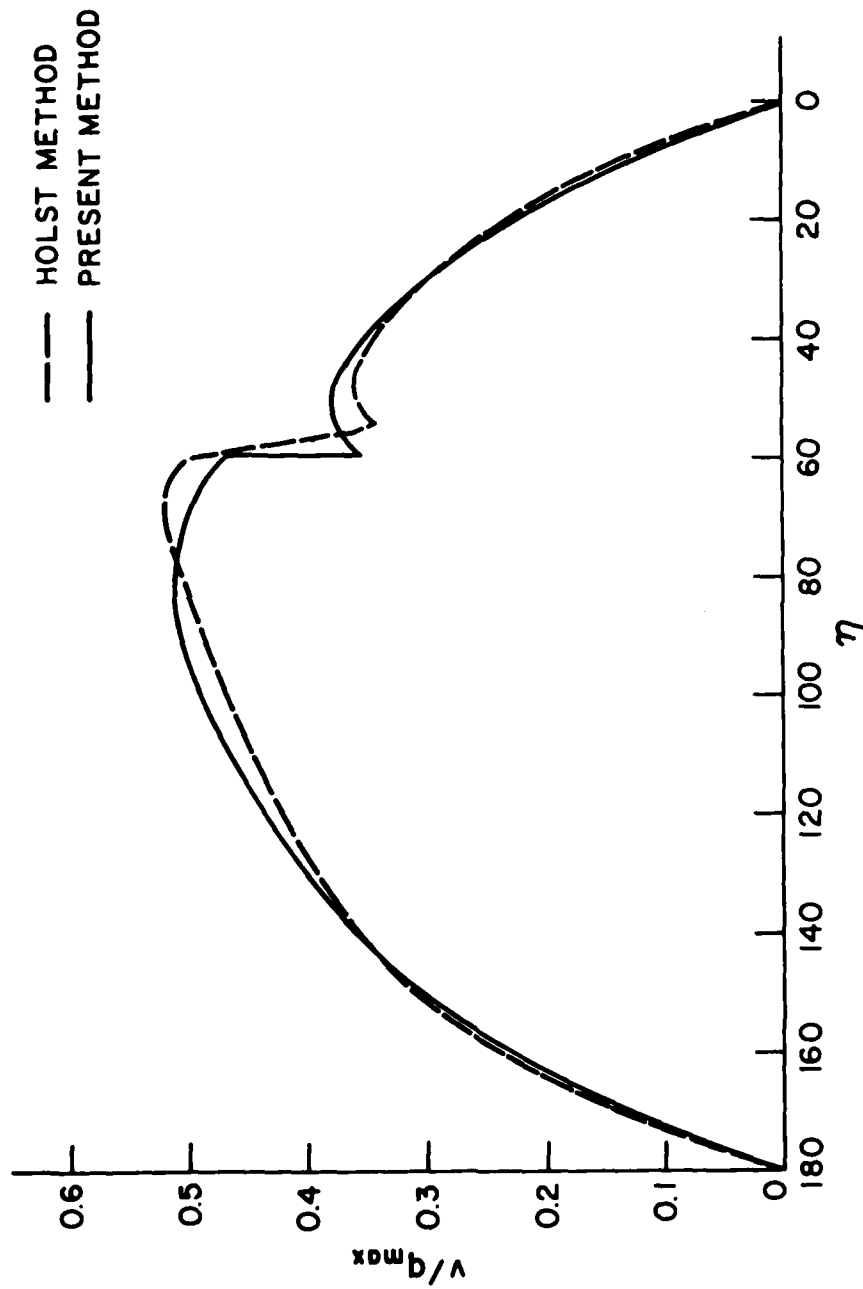


FIG. 6 SURFACE VELOCITY DISTRIBUTION. $\delta = 0.4$, $M_{\infty} = 0.65$.

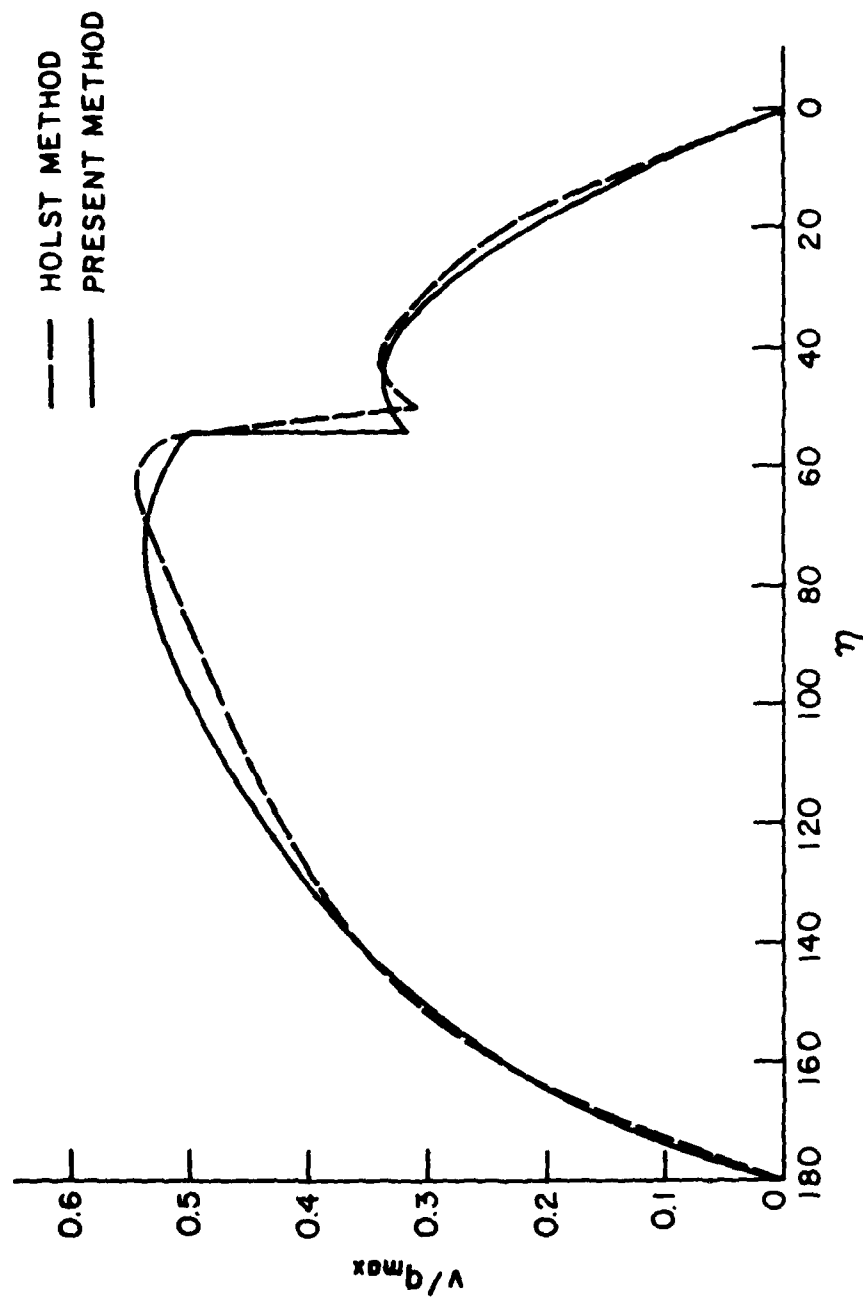


FIG. 7 SURFACE VELOCITY DISTRIBUTION. $\delta = 0.4$, $M_{\infty} = 0.66$.

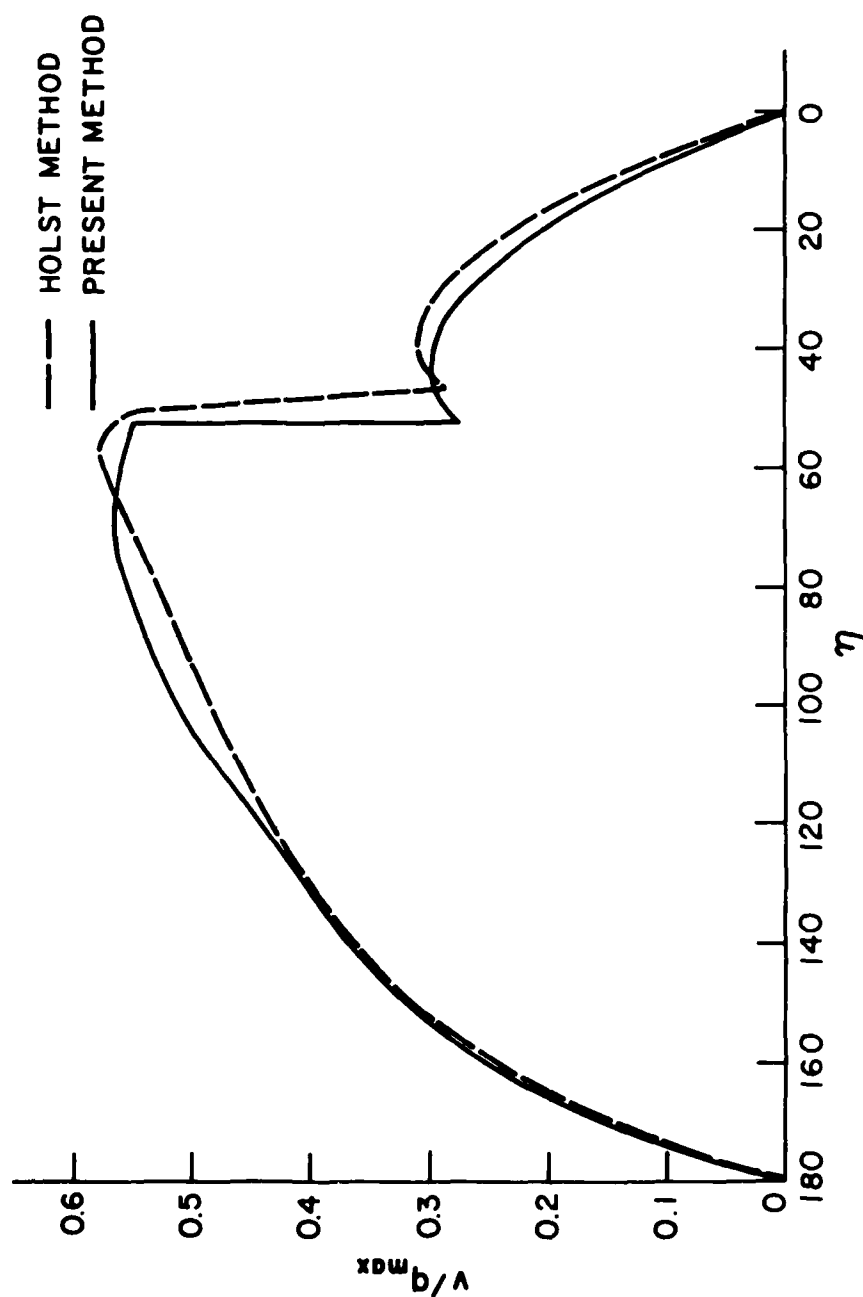


FIG. 8 SURFACE VELOCITY DISTRIBUTION. $\delta = 0.4$, $M_{\infty} = 0.67$.

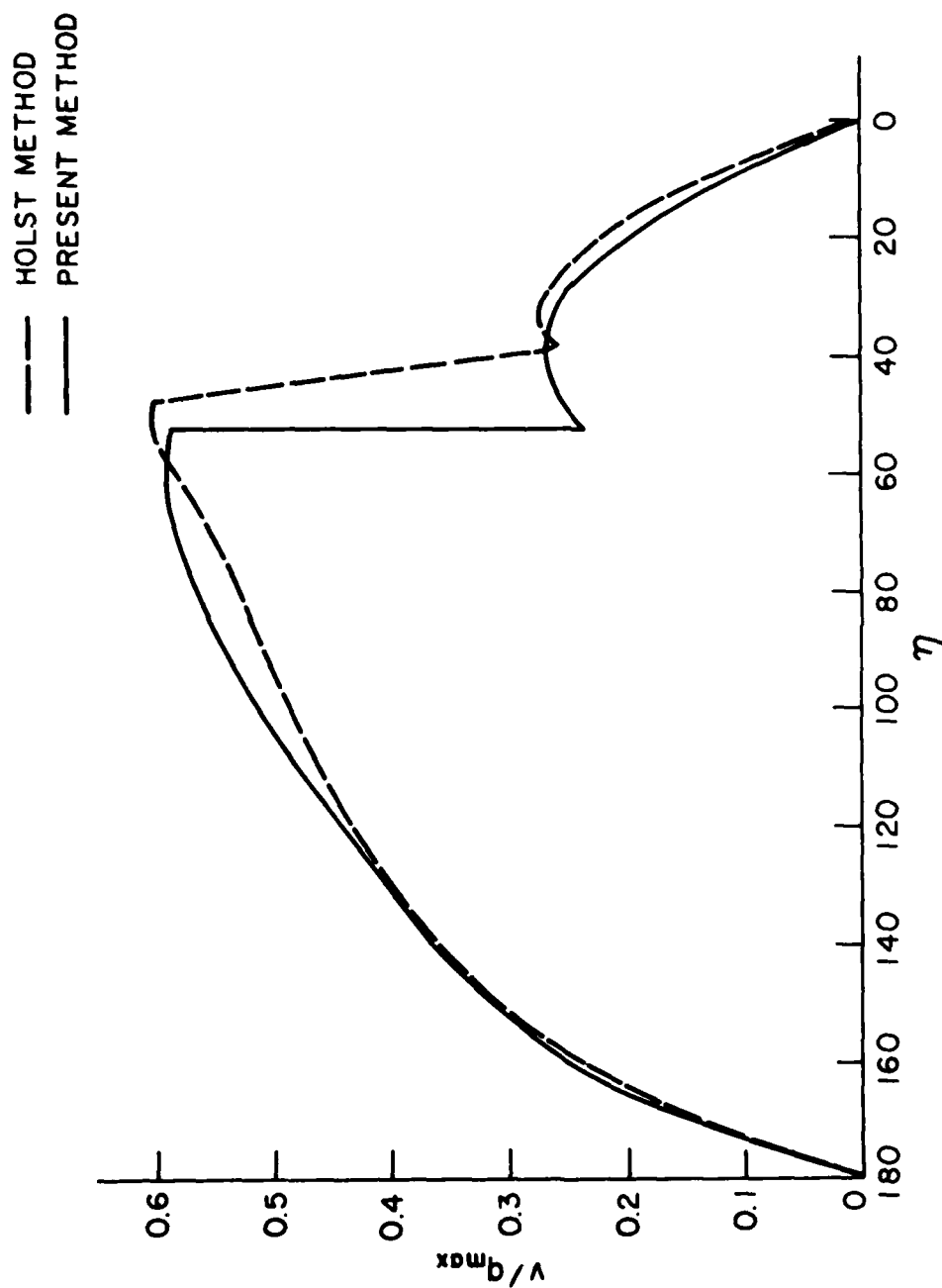


FIG. 9 SURFACE VELOCITY DISTRIBUTION. $\lambda = 0.4$, $M_{\infty} = 0.68$.

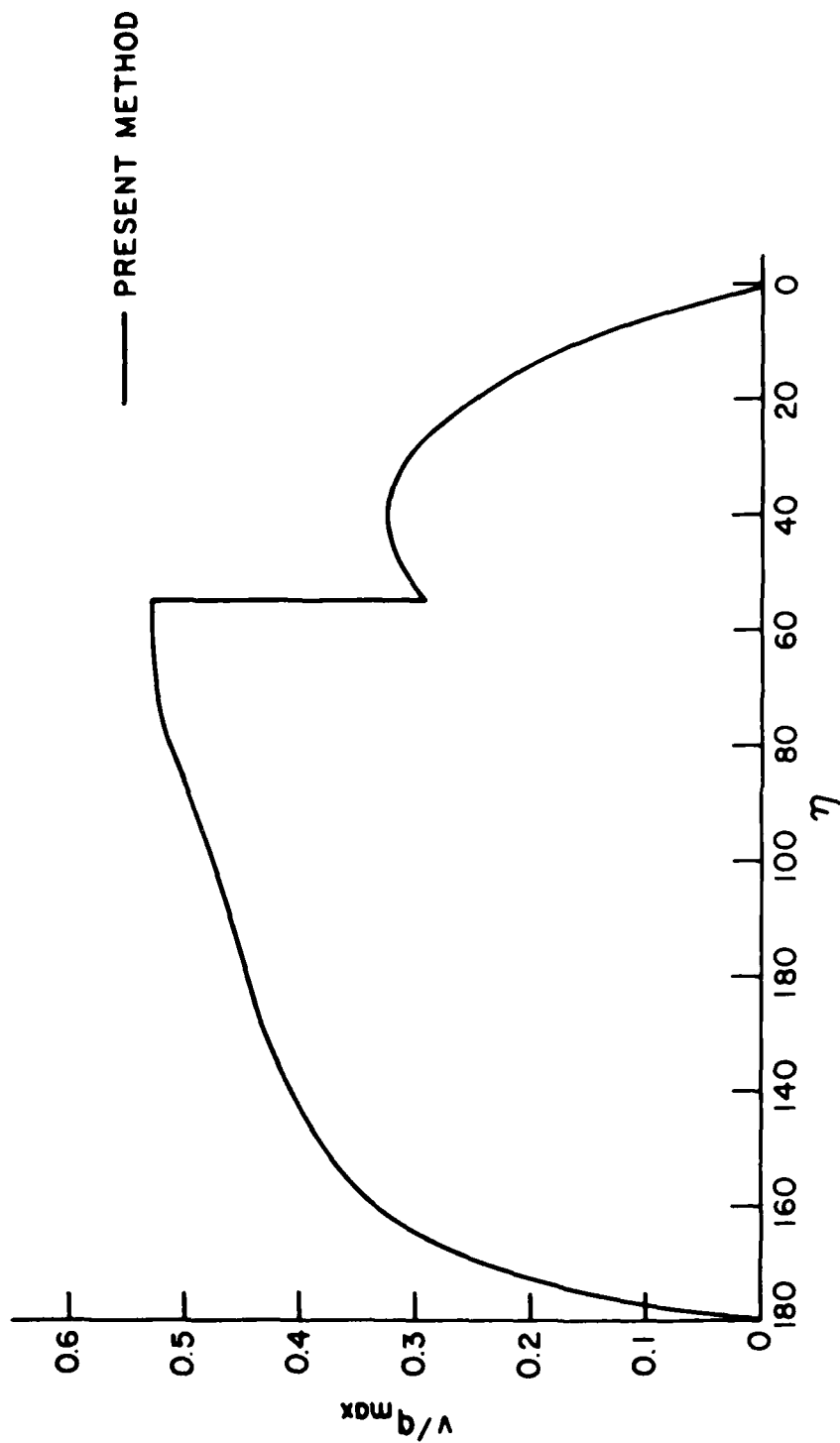


FIG. 10 SURFACE VELOCITY DISTRIBUTION. $\xi = 0.2$, $M_{\infty} = 0.77$.

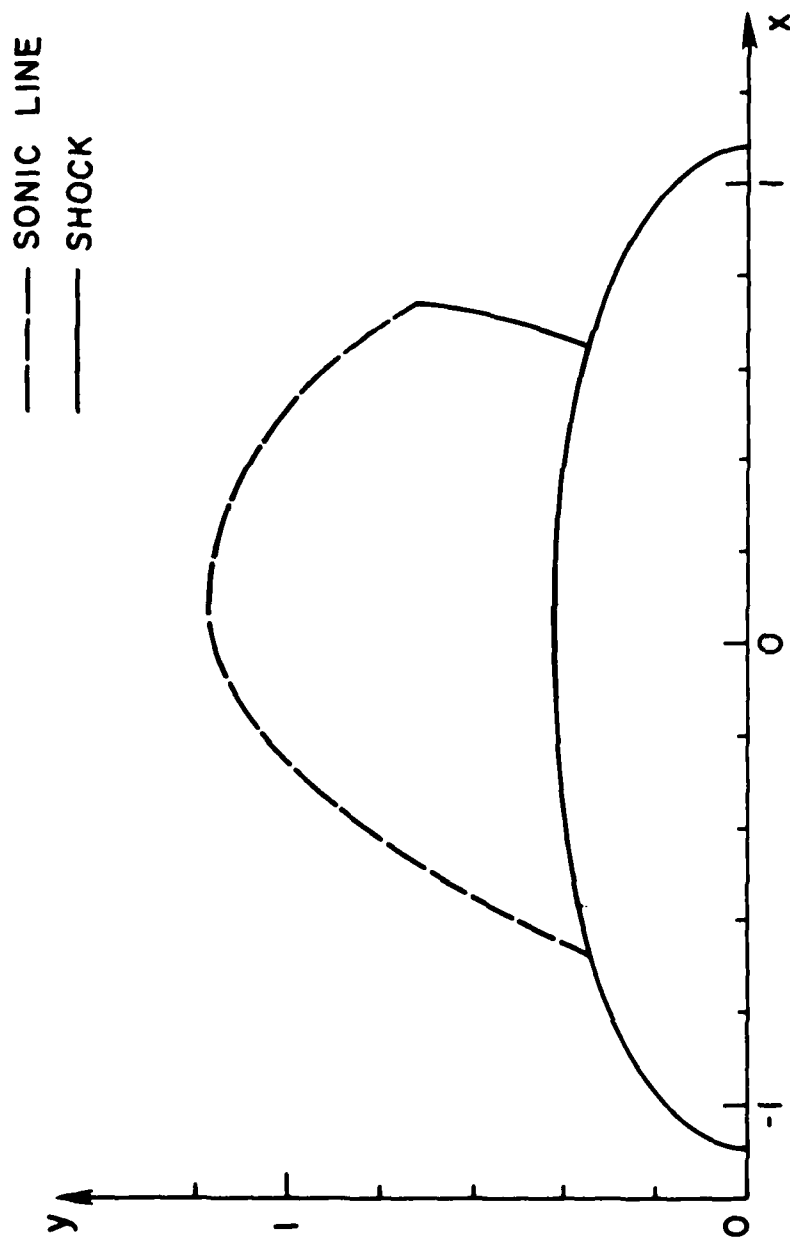


FIG. 11 BOUNDARY OF LOCAL SUPERSONIC REGION. $\delta = 0.4$, $M_{\infty} = 0.66$

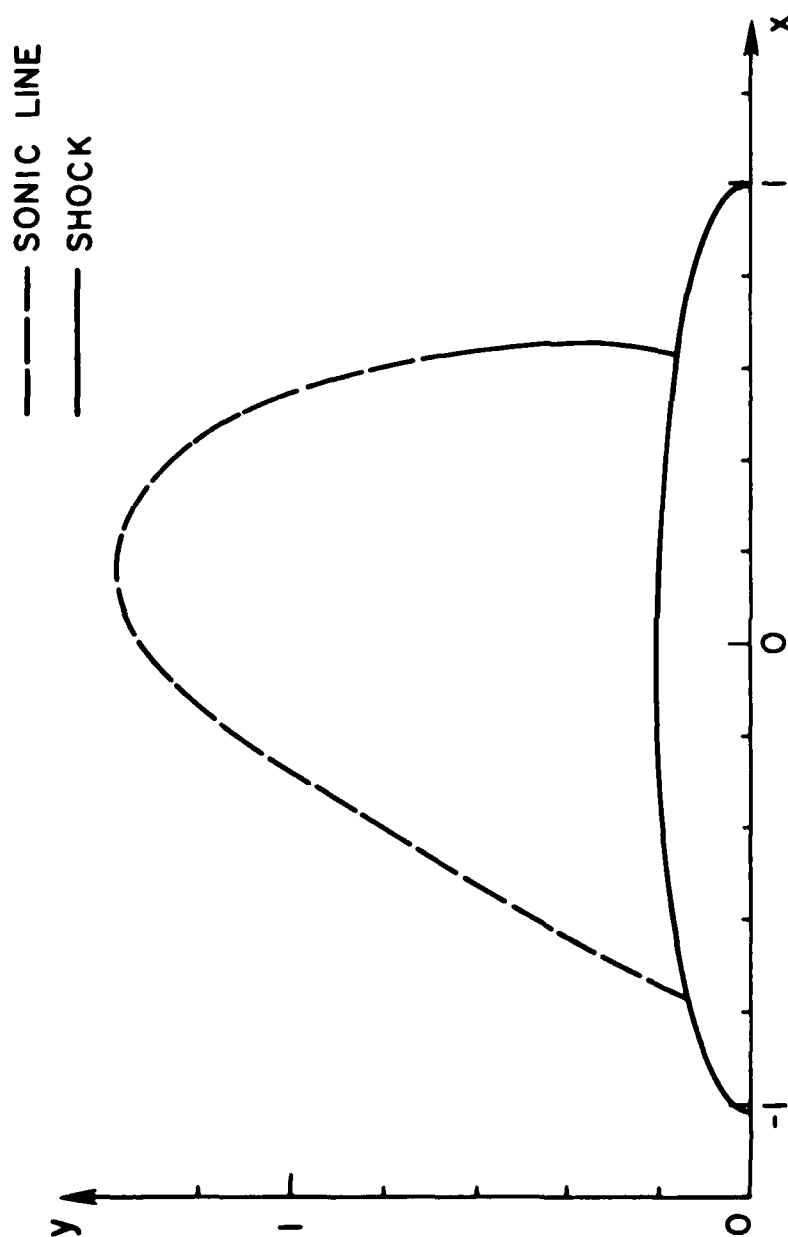


FIG. 12 BOUNDARY OF LOCAL SUPERSONIC REGION. $\delta = 0.2$, $M_\infty = 0.77$.